

RESEARCH ARTICLE

Development of follicular dendritic cells in lymph nodes depends on retinoic acid-mediated signaling

Jasper J. Koning¹, Anusha Rajaraman^{2,3}, Rogier M. Reijmers¹, Tanja Konijn¹, Junliang Pan^{2,3}, Carl F. Ware⁴, Eugene C. Butcher^{2,3,5} and Reina E. Mebius^{1,*}

ABSTRACT

Specialized stromal cells occupy and help define B- and T-cell domains, which are crucial for proper functioning of our immune system. Signaling through lymphotoxin and TNF receptors is crucial for the development of different stromal subsets, which are thought to arise from a common precursor. However, mechanisms that control the selective generation of the different stromal phenotypes are not known. Using *in vitro* cultures of embryonic mouse stromal cells, we show that retinoic acid-mediated signaling is important for the differentiation of precursors towards the *Cxcl13*^{pos} follicular dendritic cell (FDC) lineage, and also blocks lymphotoxin-mediated *Ccl19*^{pos} fibroblastic reticular cell lineage differentiation. Accordingly, at the day of birth we observe the presence of *Cxcl13*^{pos}*Ccl19*^{neg/low} and *Cxcl13*^{neg/low}*Ccl19*^{pos} cells within neonatal lymph nodes. Furthermore, ablation of retinoic acid receptor signaling in stromal precursors early after birth reduces *Cxcl13* expression, and complete blockade of retinoic acid signaling prevents the formation of FDC networks in lymph nodes.

KEY WORDS: Follicular dendritic cell, Lymph node development, Retinoic acid, Stromal cell

INTRODUCTION

Lymph nodes are strategically located to enable quick and effective interactions between antigen-presenting cells and lymphocytes leading to antigen-specific immune responses.

The non-hematopoietic stromal cells are important contributors to lymph node homeostasis as well as immune responses (Chang and Turley, 2015; Krishnamurthy and Turley, 2020). Stromal cells provide an architecture with distinct microdomains for both B and T lymphocytes, and mediate lymphocyte survival (Link et al., 2007; Mueller and Germain, 2009; Takada and Jameson, 2009) and tolerance to self-antigens (Fletcher et al., 2010; Lee et al., 2007; Magnusson et al., 2008; Nichols et al., 2007; Yip et al., 2009; Baptista et al., 2014), and, crucially, influence ongoing immune

responses (Ahrendt et al., 2008; Molenaar et al., 2009; Wolvers et al., 1999; Hammerschmidt et al., 2008; Baptista et al., 2019).

The stromal cell compartment can be subdivided into various endothelial and mesenchymal subsets (Mueller and Germain, 2009). Until recently, the major different mesenchymal stromal subsets included fibroblastic reticular cells (FRCs), marginal reticular cells (MRCs) and follicular dendritic cells (FDCs) (Chang and Turley, 2015; Koning and Mebius, 2012). Single-cell sequencing has identified additional mesenchymal stromal subtypes (Rodda et al., 2018) and shed light on the transcriptional profile of lymph node stromal cells during homeostasis and upon immune activation. Despite this increased knowledge, it remains unknown which signaling events drive the differentiation of precursor cells into these various stromal clusters.

From previous studies, we know that precursors for stromal cells, including FDCs, are already present in the mesenteric lymph nodes of newborn mice (Cupedo et al., 2004). Recently, we have shown that *nestin*^{pos} precursors give rise to the various endothelial- and mesenchymal-derived lymph node stromal cells (Koning et al., 2016).

Additional studies that specifically focused on the origin of FDCs provided evidence for the presence of local mesenchymal FDC precursors both in spleen and in lymph nodes (Castagnaro et al., 2013; Jarjour et al., 2014; Krautler et al., 2012). The presence of B cells is essential for the development of FDCs and has been shown to rely on lymphotoxin and TNF receptor signaling (Endres et al., 1999; Fu et al., 1998). The presence of perivascular precursors for FDCs in the spleen appeared to be independent of lymphotoxin signaling (Krautler et al., 2012), suggesting that a sequence of signaling events is needed for their differentiation and final maturation to become FDCs.

Here, we provide evidence that postnatal retinoic acid signaling plays a crucial role in the control of FDC development. We identify endothelial cells as an additional cellular source for the production of retinoic acid, thereby highlighting the importance of endothelial and non-endothelial stromal cells for proper development of lymph node niches. Cell-specific inhibition of retinoic acid signaling in *nestin*^{pos} precursor cells reduced *Cxcl13* expression but not FDC development. However, pharmacological inhibition of retinoic acid signaling revealed that the appearance of FDCs depends on retinoic acid signaling during neonatal lymph node development.


RESULTS

Differential stimulation via receptors for retinoic acid and lymphotoxin induces distinct gene expression profiles in mesenchymal cells *in vitro*

Lymph node development during embryogenesis involves direct crosstalk between lymphoid tissue inducer (LTi) cells and different types of stromal organizer cells (Bovay et al., 2018; Mebius, 2003; Onder et al., 2017) and requires signaling mediated by retinoic acid

¹Department of Molecular Cell Biology and Immunology, Amsterdam UMC, Vrije Universiteit Amsterdam, Amsterdam Infection and Immunity Institute, 1081HZ Amsterdam, the Netherlands. ²Laboratory of Immunology and Vascular Biology, Department of Pathology, Stanford University School of Medicine, Stanford, CA 94305, USA. ³Palo Alto Veterans Institute for Research, Palo Alto, CA 94304, USA. ⁴Infectious and Inflammatory Diseases Research Center, Laboratory of Molecular Immunology, Sanford Burnham Medical Research Institute, La Jolla, CA 92037, USA. ⁵The Center for Molecular Biology and Medicine, Veterans Affairs Palo Alto Health Care System, Palo Alto, CA 94304, USA.

*Author for correspondence (r.mebius@amsterdamumc.nl)

 J.J.K., 0000-0003-2243-4857; R.M.R., 0000-0001-7471-7715; C.F.W., 0000-0002-5006-418X; E.C.B., 0000-0001-8786-7907; R.E.M., 0000-0003-0451-7464

Handling Editor: Haruhiko Koseki

Received 14 April 2021; Accepted 9 September 2021

as well as lymphotoxin (Honda et al., 2001; van de Pavert et al., 2009). Mesenchymal cells at the presumptive lymph node site are initially exposed to retinoic acid after which $LT\alpha 1\beta 2$ -expressing LTi cells will trigger $LT\beta R$ -mediated signaling in these cells, allowing their maturation towards stromal organizer cells (van de Pavert et al., 2009). To determine whether the activity of these signaling pathways, either in sequence or on their own, could contribute to the different fates of stromal cell subsets present in adult lymph nodes, we set up *in vitro* cultures of early passage embryonic day (E) 13.5 embryonic mesenchymal cells enriched for mesenchymal stem cells (MSCs) as confirmed by their tri-lineage differentiation capacity (Fig. 1A).

Transcript analysis upon stimulation with retinoic acid alone showed strong upregulation of the β isoform of the receptor (*Rarb*), which is specifically involved in the induction of *Cxcl13* during the initiation phase of lymph node development (van de Pavert et al., 2009). Indeed, stimulation with retinoic acid induced *Cxcl13* expression in mesenchymal precursors whereas $LT\beta R$ stimulation alone did not lead to significant upregulation of *Cxcl13*, although low expression levels could be detected, as shown previously (Dejardin et al., 2002) (Fig. 1B).

$LT\beta R$ stimulation (Crowe et al., 1994) initially leads to the activation of the classical $Nf-\kappa B$ pathway (Dejardin et al., 2002; Siebenlist et al., 1994), whereas upon prolonged triggering the

alternative $Nf-\kappa B$ pathway also becomes activated resulting in the upregulation of *Ccl19*, *Ccl21* and *Il7* via nuclear localization of $RelB:p52$ dimers (Dejardin et al., 2002; Vondenhoff et al., 2009). As expected, $LT\beta R$ stimulation of mesenchymal precursors resulted in a significant upregulation of *Ccl19*, *Ccl21* and *Il7* transcripts, which are all expressed by FRC in the T-cell zone (Fig. 1C). Strikingly, cells that were first stimulated with retinoic acid and subsequently via $LT\beta R$ completely failed to induce *Ccl19*, *Ccl21* and *Il7* transcripts (Fig. 1C) but not *Cxcl13* (Fig. 1B). This inhibition was not the result of downregulation of the receptor itself, because retinoic acid stimulation changed neither mRNA expression nor cell surface expression of $LT\beta R$ (Fig. 1D,E). We also observed no difference in the activation of the non-canonical $Nf-\kappa B$ pathway, as there was similar nuclear $RelB$ translocation, but the DNA-binding capacity of nuclear $RelB$ and $p52$ ($Nfkb2$) was also not affected (Fig. S1). We observed that other $LT\beta R$ -mediated molecules, such as *VEGFC* and *MAdCAM-1* (Vondenhoff et al., 2009), were not affected by retinoic acid pre-incubation, whereas RA stimulation alone resulted in reduced *Tnfsf11* expression, which could be rescued by $LT\beta R$ stimulation (Fig. 1F).

Owing to these observations, we hypothesized that retinoic acid stimulation serves as a fate-determining signal that allows the differentiation of stromal precursor cells towards a follicular

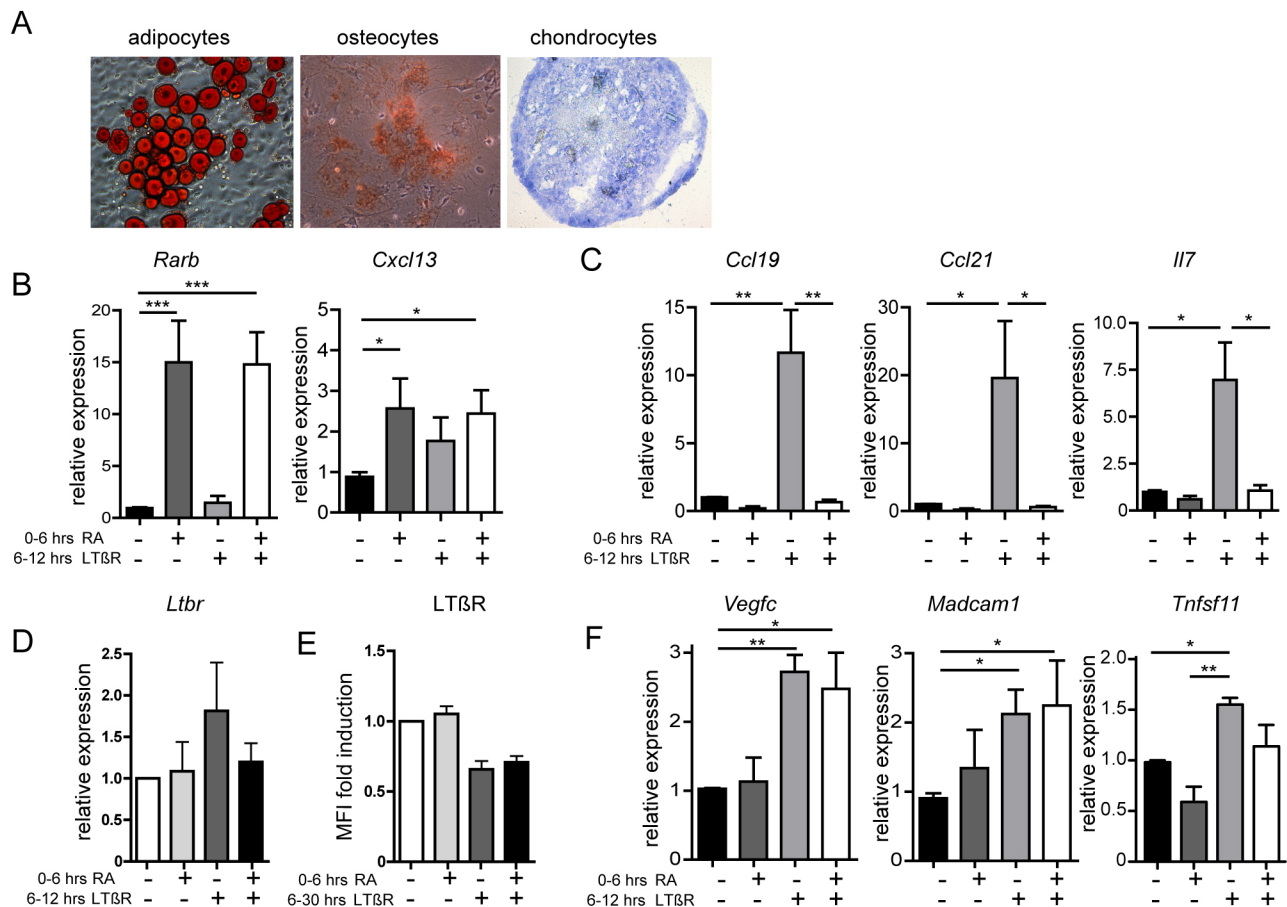


Fig. 1. Retinoic acid signaling prevents upregulation of FRC-related genes. (A) E13.5 MSCs have the capacity to differentiate into adipocytes, osteocytes and chondrocytes. (B-D,F) mRNA expression in E13.5 MSCs upon sequential stimulation with retinoic acid (RA) (6 h) followed by stimulation with $LT\beta R$ (6 h) showing expression of *Rarb* and *Cxcl13* (B), *Ccl19*, *Ccl21* and *Il7* (C), *Ltbr* (D) and *Vegfc*, *Madcam1* and *Tnfsf11* (F). (E) Flow cytometric analysis of $LT\beta R$ cell-surface expression upon stimulation with RA (6 h) followed by stimulation with $LT\beta R$ (30 h) depicted as fold induction of MFI relative to control. Data represent mean+s.e.m.; $n \geq 3$. * $P < 0.05$; ** $P < 0.01$; *** $P < 0.001$ (one-way ANOVA with Bonferroni's multiple comparison test).

dendritic cell signature by preventing their differentiation into T-cell zone FRCs upon subsequent LT β R triggering.

Localization of pre-FDCs within postnatal developing lymph nodes

Retinoic acid- and LT β R-mediated signaling takes place before birth during lymph node development. Therefore, stromal cells that have either received initially only retinoic acid-mediated signaling, versus stromal cells that received their first signals via LT β R, are potentially already present within lymph nodes at the day of birth. To investigate this, we monitored the expression of *Cxcl13* mRNA, induced by retinoic acid-mediated signaling, as well as *Ccl19*, which is expressed in the majority of stromal precursors (Chai et al., 2013) and induced upon LT β R signaling. Upon analysis of week (wk) 0 lymph nodes, we observed expression of *Ccl19* mRNA as well as *Cxcl13* mRNA within cells throughout the lymph node. Although the majority of cells expressed both molecules, cells with high expression of *Cxcl13* mRNA appeared to have low amounts of *Ccl19* mRNA, and vice versa (Fig. 2A).

We additionally monitored the expression of *Mfge8* mRNA, which is expressed by FDC precursors within the spleen, and *Tnfsf11*, which is expressed by lymphoid tissue organizer (LTO) cells as well as MRCs (Jarjour et al., 2014; Katakai et al., 2004). We observed that the majority of *Cxcl13*^{pos} cells additionally expressed *Mfge8*. The strongest levels of *Cxcl13* mRNA could be detected in cells that were located near the outer border of the lymph node and the majority of the cells expressed *Tnfsf11* mRNA as well being identified as LTO cells with MRC characteristics (Fig. 2A). At 1 week after birth, when the first clustering of B cells within lymph nodes has occurred, *Cxcl13*^{pos}*Mfge8*^{pos} cells were located within follicle areas, as well as in a large area at the outer zone of the lymph node (Fig. 2B). A substantial number of *Cxcl13*^{pos} cells also expressed *Ccl19* within the B cell follicles although the majority was negative for *Ccl19*. *Cxcl13*^{neg} cells were mostly excluded from the follicle areas and present within the developing T-cell zone where they express *Ccl19*. The majority of cells within the presumptive B-cell follicle did not express *Tnfsf11* mRNA, indicating that they are not MRCs (Fig. 2B). Within presumptive B-cell follicle areas in week 1 lymph nodes, we occasionally observed perivascular-located cells that expressed *Mfge8*, *Cxcl13* and *Ccl19* (Fig. S2A). Within readily defined B-cell follicles at week 2, we observed perivascular cells that were either *Mfge8*^{pos}*Cxcl13*^{pos} or *Mfge8*^{pos}*Ccl19*^{pos} cells (Fig. S2B). The separation between *Cxcl13*^{pos}*Ccl19*^{neg} and *Cxcl13*^{neg}*Ccl19*^{pos} cells within distinct B-cell areas versus T-cell areas became more prominent when lymph nodes matured further from 2 to 6 weeks after birth (Fig. 2C-E).

From these data, we can conclude that the cells that received retinoic acid-mediated signaling as the initial trigger during lymph node development and therefore expressed *Cxcl13* but not (or low) *Ccl19*, were indeed present within neonatal lymph nodes. With the combined expression of *Mfge8* and *Tnfsf11*, these cells have the phenotypic profile of MRCs and are already present at day of birth. Furthermore, in the developing lymph nodes at 1 week of age both *Ccl19*^{pos} cells, triggered via LT β R, as well as *Cxcl13*^{pos} cells, triggered by retinoic acid, were located within the developing B-cell follicles. *Ccl19*^{pos} cells specifically disappeared from the developing B-cell follicles in the weeks thereafter.

Multiple cellular sources of retinoic acid within lymph nodes

To determine whether retinoic acid-mediated signaling still occurs after birth and thereby could further contribute to the developing

FDC network, we investigated whether cellular sources of retinoic acid were present within neonatal lymph node. Retinoic acid synthesis depends on the two-step conversion of vitamin A into retinaldehyde and then retinoic acid. The final and irreversible step of this conversion involves members of the aldehyde dehydrogenase enzyme family – Aldh1a1, Aldh1a2, Aldh1a3 – and expression of these enzymes identifies cells that produce retinoic acid (Kedishvili, 2016). It is known that stromal cells as well as dendritic cells in adult lymph nodes express Aldh1 enzymes (Hammerschmidt et al., 2008; Molenaar et al., 2011), but their expression during early postnatal lymph node development has not been studied before.

Therefore, we used flow cytometric cell sorting to sort the three main stromal subsets – FRCs, blood vascular endothelial cells (BECs) and lymphatic endothelial cells (LECs) – as well as dendritic cells (CD11c^{high}MHCII^{high}) from the peripheral lymph nodes (pLNs) of 1-week-old and 2-week-old mice, to examine the expression of Aldh1 enzymes. Dendritic cells are known to express high levels of Aldh1a2 (Zhang et al., 2016) and transcriptomic analysis indeed showed that dendritic cells expressed the highest level of *Aldh1a2* at both time points in pLNs but lacked both *Aldh1a1* and *Aldh1a3* expression. Sorted FRCs expressed both *Aldh1a1* and *Aldh1a3* but not *Aldh1a2*. The expression of *Aldh1a1* was higher in week 2 sorted FRCs. To our surprise, we found that BECs also express *Aldh1a1*, whereas LECs express *Aldh1a3* (Fig. 3A, Fig. S3).

Because lymph node BECs are not recognized as Aldh1-expressing cells, we wanted to verify the expression at the protein level. We therefore performed immunofluorescence on postnatal developing lymph nodes and could show the expression of Aldh1a1 in BECs. Within BECs, Aldh1a1 expression could be detected already at the day of birth (Fig. 3B) and was abundantly present in BECs at day 7 after birth (Fig. 3C). Upon analyzing Aldh1a1 enzyme expression over time, we observed weak Aldh1a1 expression in BECs in lymph nodes of 6-week-old mice (Fig. 3D). At that time, we observed Aldh1a1 expression in a subset of FDCs in B-cell follicles. This expression was only seen in lymph nodes of adult mice (Fig. S3).

Together, these data indicate that during early postnatal lymph node development, Aldh1 enzymes are expressed by multiple cell types, all of which could serve as cellular sources of retinoic acid that potentially mediate further FDC development.

Postnatal abrogation of retinoic acid signaling in nestin-expressing precursors does not prevent FDC formation

The multicellular distribution of retinoic acid-producing enzymes prevents clarification of the importance of each of these cellular sources for postnatal FDC development as the functional consequences of cell-specific Aldh1 deletion in one cell subset, could be rescued by the expression of another Aldh1 enzyme in the same cell type (or by the expression of the same and other enzymes in another subset).

However, cell-specific ablation of retinoic acid receptor signaling in precursor cells could be used to study the importance of retinoic acid signaling for further postnatal FDC development. Although the precursor(s) for FDCs within neonatal lymph nodes have not been identified so far, we have shown in the past that nestin-expressing cells can give rise to FDCs (Koning et al., 2016). We reasoned that ablation of retinoic acid receptor signaling in these cells shortly after birth would impact further FDC development. We performed cell-specific ablation of retinoic acid receptor signaling in nestin-expressing cells by crossing Nes-Cre^{ERT2} mice with dominant-

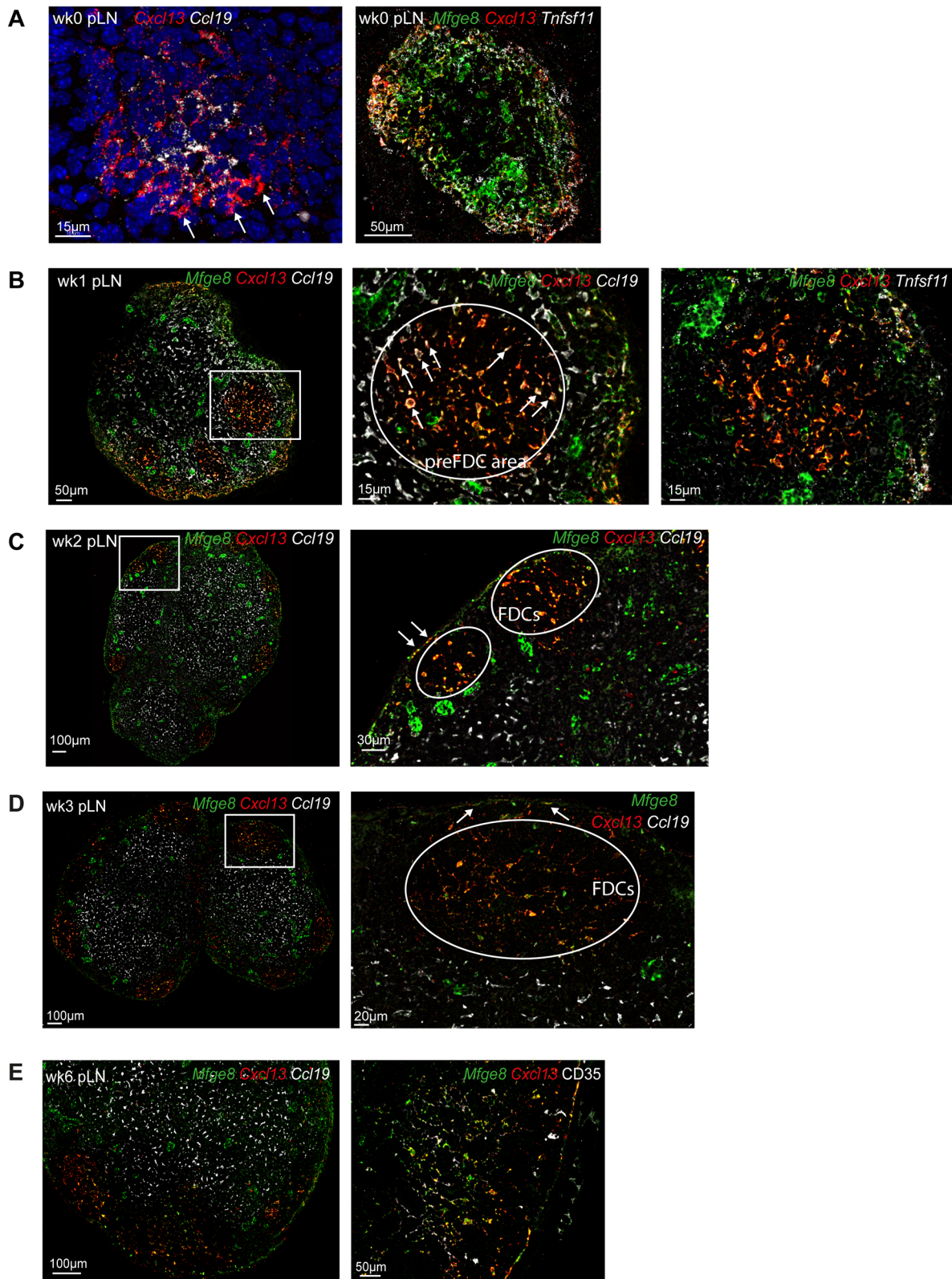


Fig. 2. Localization of FDC precursors. (A-E) Confocal analysis of multiple fluorescence *in situ* hybridizations at different time points after birth in pLNs. (A) Combined expression of *Cxcl13* and *Ccl19* (left) or *Mfge8*, *Cxcl13* and *Tnfsf11* (right) in pLNs at the day of birth. Arrows indicate cells expressing high levels of *Cxcl13* and low levels of *Ccl19*. (B) Combined expression of *Mfge8*, *Cxcl13* and *Ccl19* (left and middle) and *Mfge8*, *Cxcl13* and *Tnfsf11* (right) in lymph nodes at 1 week after birth. Arrows indicate *Mfge8*^{pos}*Cxcl13*^{pos}*Ccl19*^{pos} cells in the preFDC area. (C,D) Expression of *Mfge8*, *Cxcl13* and *Ccl19* in lymph nodes at week 2 (C) and week 3 (D) after birth. Arrows indicate MRCs. (E) *Mfge8*, *Cxcl13* and *Ccl19* expression (left) and *Mfge8*, *Cxcl13* and *Cd35* expression (right) in lymph nodes at 6 weeks after birth. Data are representative of at least $n=3$ individual mice per time point. In B-D, panels to the right show magnifications of the boxed areas to the left, and FDC areas are encircled.

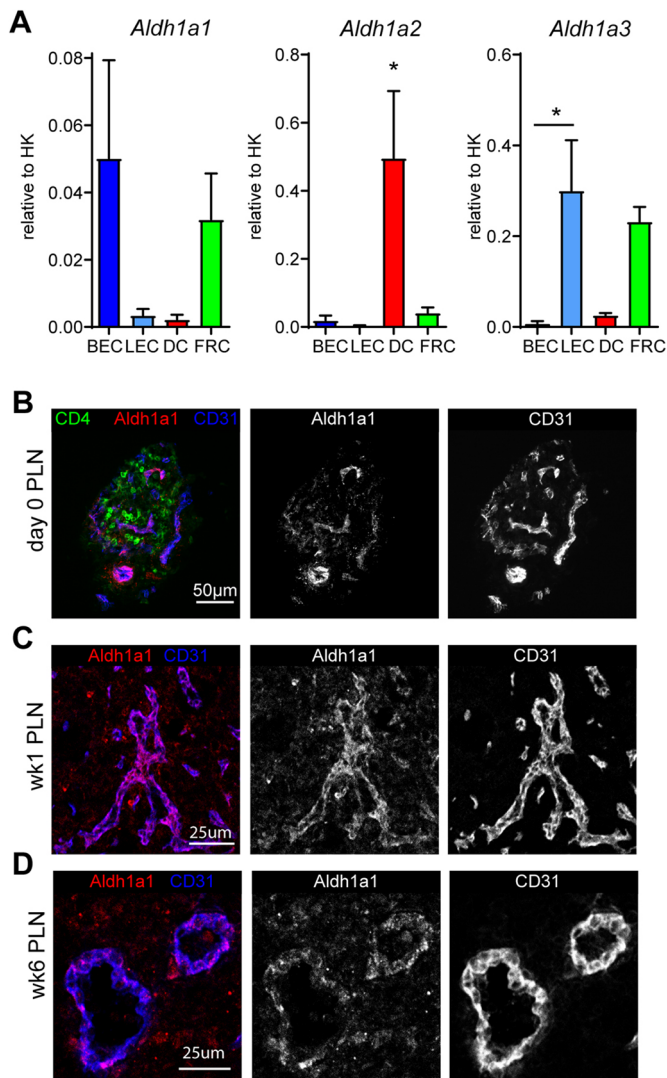


Fig. 3. Multiple cellular sources of Aldh1 enzymes. (A) mRNA expression levels of *Aldh1a1-3* relative to housekeeping genes (HK) in sorted stromal cells and dendritic cells of week 1 pLNs. (B-D) Immunofluorescence analysis of Aldh1a1 expression in week 0 (B), wk1 (C) and wk6 (D) pLNs. $n=3$. Error bars represent s.e.m.

negative RAR (RAR-dn) mice in order to abrogate retinoic acid signaling specifically in nestin-expressing cells upon tamoxifen treatment. Animals were treated from day 5 after birth for 5 consecutive days and lymph nodes were isolated when the animals were 2 or 3 weeks old.

Upon transcriptomic analysis of whole lymph nodes, we observed no difference in the mRNA expression of *Rarb* (Fig. S4C,F) most likely because only a small subset of cells was targeted. mRNA expression of *Cxcl13*, however, was reduced in the pLNs of 2-week-old animals (Fig. 4A). This was mainly attributed to a reduction of *Cxcl13* expression in axillary and brachial lymph nodes because similar levels of *Cxcl13* were found in inguinal lymph nodes of mice that were Nes-Cre^{ERT2} negative (Fig. S4A). Because CD35^{pos} FDCs were not present yet in both experimental groups, we analyzed the size of the B-cell follicles, which showed no differences between lymph nodes from both groups (Fig. 4B). In order to see whether FDCs would develop, we examined mice that were left untreated for 3 weeks after the 5-day tamoxifen treatment. We observed no differences in *Cxcl13* mRNA expression (Fig. 4C)

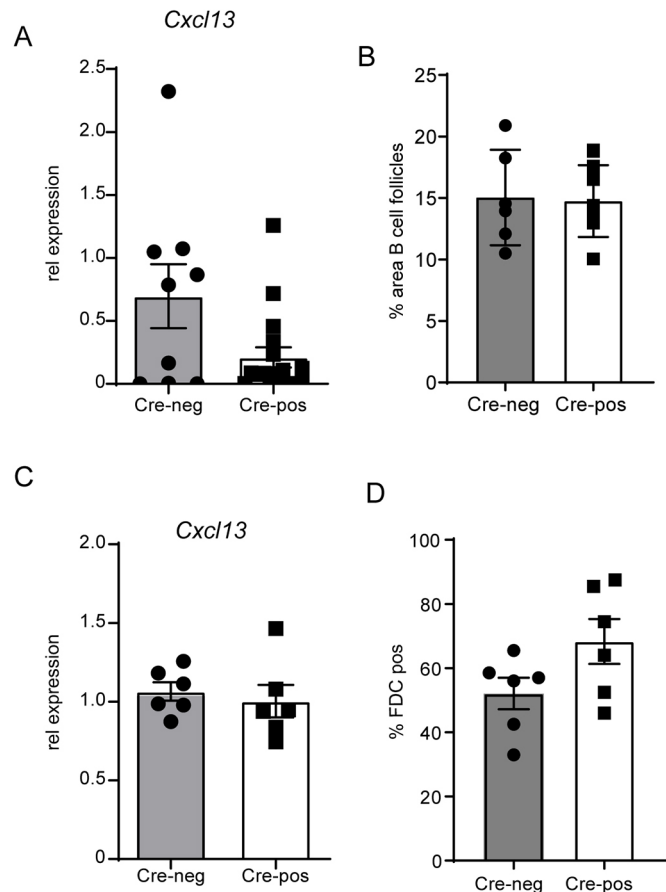


Fig. 4. Retinoic acid receptor signaling blockade in nestin precursors does not prevent FDC formation. (A,C) Relative *Cxcl13* mRNA expression in pLNs of Nes-Cre^{pos}×RarDN mice compared with Nes-Cre^{neg}×RarDN littermates. (B) Quantification of B-cell areas in pLNs of 2-week-old Nes-Cre^{pos}×RarDN mice compared with Nes-Cre^{neg}×RarDN littermates. (D) Quantification of the percentage of FDC-positive B-cell follicles in pLNs of 3-week-old Nes-Cre^{pos}×RarDN mice compared with Nes-Cre^{neg}×RarDN littermates. Data represent mean±s.e.m.; $n \geq 3$. * $P < 0.05$ (unpaired Student's *t*-test).

and upon histological analysis FDCs could be found within B-cell follicles of both groups (Fig. 4D).

Based on these observations, we can conclude that deletion of retinoic acid signaling specifically in nestin-expressing precursor cells shortly after birth does not result in blockade of FDC development.

Early postnatal blockade of retinoic acid receptor signaling prevents FDC development

In order to block all retinoic acid signaling and address whether retinoic acid-mediated signaling is involved in FDC development postnatally, we performed pharmacological inhibition of retinoic acid receptor signaling using oral application of BMS493 (Mizee et al., 2013; van de Pavert et al., 2014) from postnatal day 4 onwards for 7 or 10 consecutive days.

As expected, transcript levels of *Rarb* were downregulated in peripheral as well as mesenteric lymph nodes upon BMS493 treatment at both time points, indicating effective blockade of retinoic acid signaling (Fig. 5A, Fig. S5D). As a consequence, mRNA levels of *Cxcl13* were also reduced and we hardly observed CXCL13 protein expression in B-cell areas and subcapsular sinuses of pLNs (Fig. 5B,C). Importantly, other transcripts related to T-cell

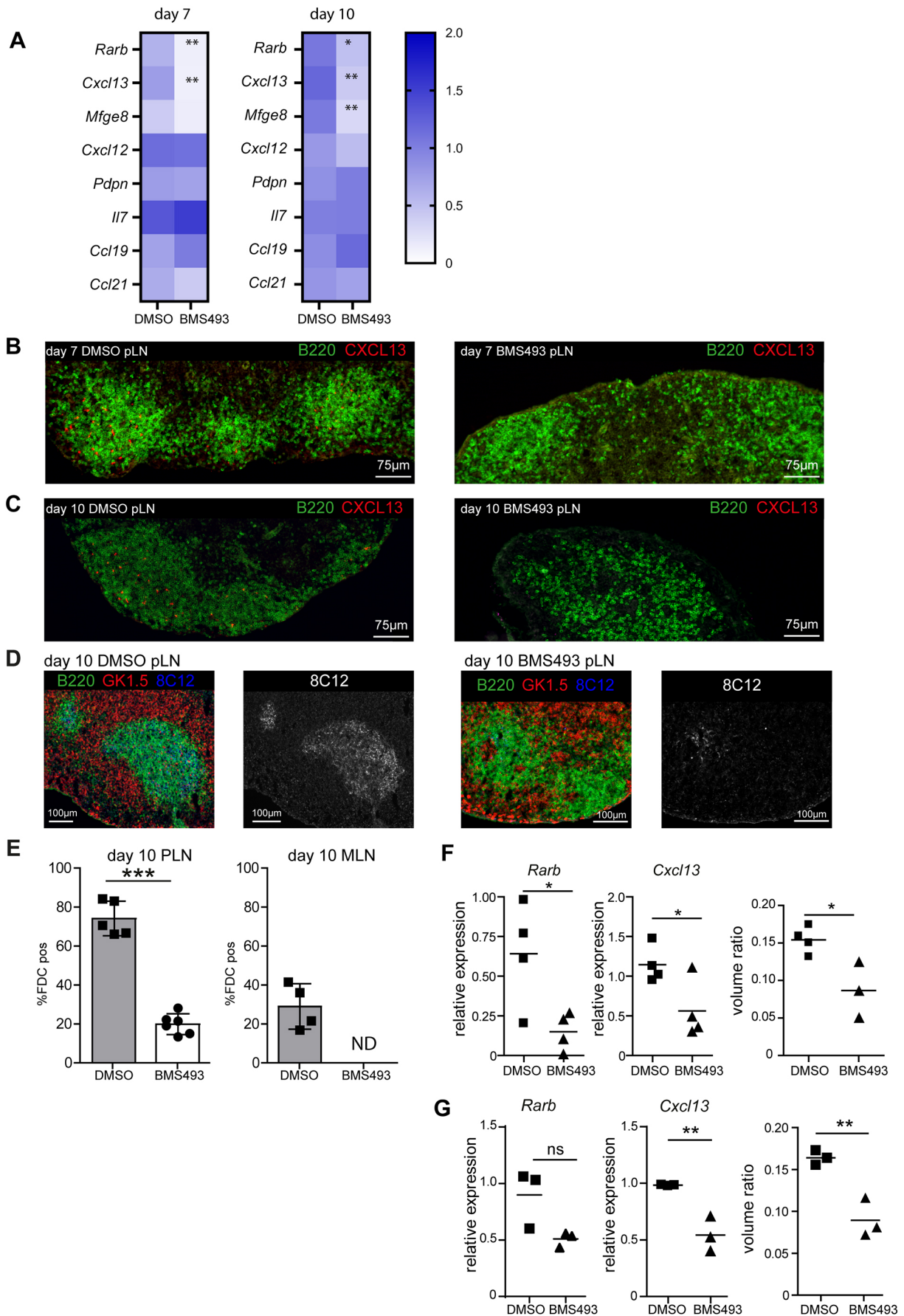


Fig. 5. See next page for legend.

Fig. 5. Inhibition of retinoic acid receptor signaling prevents CXCL13 expression and development of FDCs in lymph nodes. (A) Heatmap showing mRNA expression levels of the listed genes in pLNs upon treatment for 7 and 10 days with BMS493, starting at day 4 after birth. (B,C) Immunofluorescence analysis of CXCL13 protein expression (in red) in peripheral lymph nodes of DMSO (control) and BMS493-treated mice at day 7 (B) and day 10 (C) after the start of treatment (age of mice is 11 and 14 days, respectively). (D,E) Immunofluorescence analysis of FDCs (8C12 in blue) in pLNs (D) and quantification of FDCs in lymph nodes (E) of DMSO (control) and BMS493-treated animals at day 10 after treatment. (F,G) mRNA expression levels of *Rarb* and *Cxcl13* and volume ratio of B-cell follicle volume over total lymph node volume in pLNs of mice that were treated for 14 days with suboptimal doses of BMS493 versus DMSO (F) or for 7 days with BMS493 versus DMSO and left untreated for 21 days (G) starting at day 4 after birth. Data represent mean \pm s.e.m.; $n \geq 3$. * $P < 0.05$; ** $P < 0.01$; *** $P < 0.001$ (unpaired Student's *t*-test). ns, not significant ($P > 0.05$).

zone stromal cells, such as *Ccl19*, *Ccl21*, *Pdpr* (podoplanin), *Cxcl12* and *Il7*, were not decreased upon blockade of retinoic acid receptor signaling, indicating normal development of the other stromal cell subsets (Fig. 5A). In mesenteric lymph nodes, we even observed increased levels of *Ccl19* (Fig. S5D). As *Mfge8* has been identified as a marker for FDC precursors in the spleen (Krautler et al., 2012), we checked for its expression upon blockade of retinoic acid receptor signaling and observed that transcript levels were reduced only in pLNs after 10 days of BMS493 treatment (Fig. 5A).

Most importantly, inhibition of retinoic acid receptor signaling by BMS493 treatment almost completely prevented the development of CD35^{pos} FDC networks in B-cell areas in both peripheral and mesenteric lymph nodes (Fig. 5D,E). In mesenteric lymph nodes, inhibiting retinoic acid receptor signaling prevented the development of FDCs completely, and in pLNs the percentage of B-cell follicles that contained FDCs were significantly reduced (Fig. 5E).

The absence of *Cxcl13* expression and FDC networks severely affected B-lymphocyte organization. In both peripheral and mesenteric lymph nodes of BMS493-treated mice, the number of B-cell follicles that had formed at day 10 was lower compared with controls (Fig. S5C,E).

Within the spleen, *Rarb* transcripts were also reduced as a result of BMS493 treatment. At day 7, this resulted in a reduced level of *Cxcl13*, whereas at 10 days after treatment *Cxcl13* levels were not different from those of control mice (Fig. S5F). Immunofluorescence analysis revealed development of FDC networks in spleens from BMS493-treated mice (Fig. S5G), suggesting different signaling requirements for FDC development in spleen compared with lymph nodes.

To reduce, but not completely block, retinoic acid-mediated signaling, we provided suboptimal doses of BMS493 starting at postnatal day 4 for 14 consecutive days. This treatment resulted in lower *Rarb* and *Cxcl13* transcript levels (Fig. 5F) and we could detect low levels of CXCL13 protein in the B-cell follicles as well as FDC networks although they appeared smaller (data not shown). Whole lymph node imaging using light-sheet microscopy revealed that the total lymph node volume as well as the B-cell follicle volume in suboptimal BMS493-treated peripheral lymph nodes were lower compared with control lymph nodes, with a lower percentage of the lymph node volume being occupied by B-cell follicles (ratio of B cell area/total lymph node area) (Fig. 5F, Fig. S5H,I). We observed similar results when we blocked FDC development for 7 days and left the mice untreated for 21 days (Fig. 5G, Fig. S5J).

In summary, these data demonstrate the requirement of retinoic acid receptor signaling for postnatal development of FDCs within lymph nodes.

DISCUSSION

Our results show the importance of retinoic acid signaling for the postnatal development of FDCs and, consequently, B-cell follicle formation in adult mouse lymph nodes.

Previous research has shown that lymphotoxin- as well as TNF α -mediated signaling is a prerequisite for the presence and maintenance of mature FDCs (Endres et al., 1999; Fu et al., 1998). Lymphotoxin signaling is not exclusively required for the differentiation and subsequent maintenance of FDCs as FRCs and MRCs also depend on signaling via this pathway (Roozendaal and Mebius, 2011). This suggests that additional signaling events are needed for precursors to develop into the various stromal subsets. Because retinoic acid plays a crucial role in the initiation of lymph node development before lymphotoxin-mediated signaling takes place, we hypothesized that retinoic acid signaling could be important for the early differentiation of mesenchymal precursors towards different stromal subsets as well.

Indeed, our results from *in vitro*-stimulated mesenchymal-derived precursors showed that retinoic acid prevented the expression of transcripts that are normally induced upon LT β R signaling through activation of the non-canonical NF- κ B pathway, and that are associated with FRCs (Dejardin et al., 2002). It has been shown previously that administration of retinoic acid leads to reduced NF- κ B activity *in vivo* without affecting p65 (RelA) DNA-binding capacity (Austena et al., 2004). We show here that retinoic acid selectively inhibits transcripts associated with T-cell stroma, expression of which depends on the activation of the non-canonical NF- κ B pathway, without affecting RelB or p52 DNA-binding capacity. Furthermore, *Cxcl13* expression in mesenchymal precursors was unaltered upon sequential stimulation with retinoic acid and LT β R, suggesting a role for retinoic acid in favoring differentiation towards B-cell stroma.

By blocking retinoic acid signaling *in vivo*, we were able to prevent the development of FDCs in lymph nodes, which has been shown to depend on lymphotoxin- and TNF α -mediated signaling. Together, our data point to a model in which mesenchymal precursor cells for FDCs are sequentially triggered, first by retinoic acid and subsequently by lymphotoxin and TNF α to finally differentiate towards FDCs.

This fate-determining process potentially takes place before birth, as *Cxcl13*^{high}*Ccl19*^{neg/low} cells could be observed already at the day of birth, indicating that differentially activated lymph node stromal cells are already present. Of interest is the observation that within developing B-cell follicles both *Cxcl13* single-positive and *Cxcl13*/*Ccl19* double-positive cells were identified. Upon further development, these *Cxcl13*/*Ccl19* double-positive cells seem to disappear from the B-cell follicles. Also after birth, retinoic acid signaling seems to be crucial for proper FDC development, as postnatal blockade with pharmacological inhibitors prevented development of FDC networks. Although we could not prevent the appearance of *Cxcl13*^{pos} cells upon postnatal BMS493 treatment, owing to their presence already at day of birth, their final maturation into mature FDCs was prevented. This suggests that after birth retinoic acid signaling is a prerequisite for final FDC differentiation. Identifying the molecular mechanism of retinoic acid-specific repression of chemokine and cytokine signaling in precursor stromal cells would be extremely interesting. It is possible that retinoic acid-mediated signaling specifically prevents access of RelB

to particular promoter regions, thereby regulating the transcription of FRC-specific genes, although this requires further study.

This neonatal fate-determining step takes place when precursors are in close association with cells expressing Aldh1 enzymes, including dendritic cells, (lymphatic) endothelial cells as well as mesenchymal stromal cells.

In the absence of retinoic acid-mediated signaling, precursors can still differentiate towards T-cell stromal cells upon LT β R-mediated signaling. Indeed, in the scenario in which retinoic acid-mediated signaling was blocked, FDC and B-cell follicles failed to develop but expression of FRC-related chemokines was detected at normal levels in stromal cells.

Within secondary lymphoid organs, expression of Aldh1 enzymes has been reported in gut-derived dendritic cells (DCs), lymph node stromal cells in mesenteric lymph nodes and epithelial cells in Peyer's patches (Molenaar et al., 2011; Suzuki et al., 2010; Zhang et al., 2016). In addition, we identified endothelial cells, both high endothelial venules (HEVs) and lymphatic endothelial cells (LECs), as cells that transiently express Aldh1 enzymes most prominently during the period in which lymph nodes expand and stromal subsets are being formed. The observed decrease in Aldh1 expression after this period of expansion suggests that the differentiation of mesenchymal precursors towards the B-cell stromal lineage occurs within a postnatal timeframe. Whether endothelial cells re-express Aldh1 enzymes upon activation when FDC networks remodel and new FDCs are needed (Jarjour et al., 2014) has not been studied.

It is not known how Aldh1 expression in neonatal lymph nodes is induced but (hematopoietic) cell subsets such as the neo-migratory DCs (Zhang et al., 2016) could be involved. These cells express Aldh1 enzymes themselves and induce maturation of HEVs as their arrival in gut as well as skin draining lymph nodes leads to increased amounts of PNA α (NTAN1) expression in HEVs. This migration depends on commensal fungi and the absence of microbiota clearly affects their presence in pLNs (Zhang et al., 2016). Whether neo-migratory DCs are involved in inducing Aldh1 expression in HEVs and LECs and whether retinoic acid produced by these DCs are in fact instrumental for this effect is unknown. However, the blockade of retinoic acid signaling that prevented FDC development in the experiments presented here occurred before the entry of neo-migratory DCs in skin-draining lymph nodes, which is around 2 weeks after birth, suggesting that they are not involved (Zhang et al., 2016). It remains to be determined which of the ALDH-expressing cell types is/are the key source for retinoic acid production that mediates FDC development after birth. This would require deletion of multiple retinoic acid-producing enzymes in specific cell types shortly after birth.

Although FDCs were first described many years ago (Mitchell and Abbot, 1965), the discovery of their precursors in lymphoid organs has remained elusive until recently. Whereas in the spleen specific precursors for FDCs have been documented in several reports (Castagnaro et al., 2013; Krautler et al., 2012), progenitor-progeny relationships for lymph nodes are not so clear yet. Lineage-tracing studies showed MRCs at least in part to be precursors for FDCs (Jarjour et al., 2014). Other models have shown that upon neonatal lineage tracing of lymphoid tissue organizer cells, a subset of these cells give rise to MRCs, but not to FDCs (Hoorweg et al., 2015). In addition, as mentioned by Jarjour et al. (2014), other precursors for FDCs may exist. In the spleen, precursors for FDCs can be identified based on the expression of *Mfge8* and *Cxcl13* and these cells are perivascular located. Here, we show that also in neonatal lymph nodes, *Mfge8*^{pos}*Cxcl13*^{pos} cells can already be

identified at the day of birth throughout the lymph node, and over time these cells start to localize in B-cell follicles as well as in the subcapsular sinus. In adult lymph nodes, the majority of these cells can be detected by the expression of CD35 (CR2), a marker for FDCs, indicating that lymph node FDC precursors can be identified by similar markers as well. However, in adult lymph nodes, we did not detect *Mfge8*^{pos}*Cxcl13*^{pos} cells surrounding blood vessels. This could mean that either precursors for FDCs are not located in the perivascular space or that they do not express these markers upon homeostasis.

Our results allow for a lineage tree model in which precursors, upon encounter with retinoic acid and subsequent stimulation with lymphotoxin, will become a functional FDC, whereas in the absence of retinoic acid-mediated signaling they differentiate towards the FRC fate.

MATERIALS AND METHODS

Mice

C57BL/6 were bred and maintained at the Amsterdam Animal Research Center (AARC) under specific pathogen-free conditions. The Animal Experiments Committee of the VU (Vrije Universiteit) University Medical Center approved all of the experiments described in this study. RAR DN403 (a kind gift of Dr S. Sockanathan, Department of Neuroscience, Johns Hopkins School of Medicine, Baltimore, USA; Rajaii et al., 2008) and Nes-cre^{ERT2} [C57BL/6-Tg(Nes-cre/ERT2)4Imayo; Imayoshi et al., 2006] mice were bred and maintained at Palo Alto Veterans Institute of Research, Palo Alto, USA. To block retinoic acid receptor signaling postnatally in nestin-expressing cells, tamoxifen was dissolved in corn oil (Sigma-Aldrich, C8267) at a final concentration of 10 mg/ml and mothers were treated via oral gavage with 1 mg tamoxifen (Sigma-Aldrich, T5648) per day for 5 consecutive days, starting at day 5 after delivery.

BMS493 treatment

For *in vivo* blockade of retinoic acid signaling, mice were treated with the pan-retinoic acid receptor antagonist BMS493 (5 mg/kg; Tocris Bioscience) or vehicle (DMSO) in corn oil as described before (van de Pavert et al., 2014). Mice were treated for 7 or 10 days via oral gavage twice daily with 10-12 h intervals starting at day 4 after birth. After 7 or 10 days, mice were sacrificed for analysis. For temporal blockade of retinoic acid signaling, mice were treated the same way for 7 days and left untreated for another 21 days after which they were sacrificed for analysis. For suboptimal blockade of retinoic acid signaling, mice received 2.5 mg/kg BMS493 or vehicle (DMSO) for 14 days.

Single-cell suspensions

E13.5 mesenchymal cells were prepared as described (van de Pavert et al., 2009). In short, the head, extremities and organs were removed from E13.5 embryos and the remaining tissue was enzymatically digested with Blendzyme 2 (0.5 mg/ml; Roche Applied Sciences), DNA-se I (0.2 mg/ml; Roche) in PBS for 15 min at 37°C with continuous stirring. Cell suspensions were washed with RPMI supplemented with FCS (2%) as well as antibiotics and counted. Subsequently, cells were cultured in Mesencult proliferation medium [Mesencult Basal Medium supplemented with MSC stimulatory supplements (STEMCELL Technologies) and 2% antibiotics and glutamine]. Upon their second passage, cells were used for experiments.

Lymph node single-cell suspensions were made according to the following protocol. Isolated peripheral lymph nodes (which include axillary, brachial and inguinal lymph nodes) as well as mesenteric lymph nodes were pierced with a 25 g needle and placed in RPMI-1640 on ice. Upon start of digestion, lymph nodes were transferred to a tube containing 2 ml freshly prepared digestion medium (RPMI-1640) containing 0.8 mg/ml Dispase II, 0.2 mg/ml collagenase P and 0.1 mg/ml DNA-se I (all from Roche). Tubes were incubated at 37°C for 20 min and gently vortexed every 5 min. After 20 min, suspensions were gently pipetted to break the lymph node capsule. Upon settlement of large fragments, supernatant was transferred to a collection tube containing 10 ml ice-cold

FACS-buffer (2% FCS, 5mM EDTA in PBS) and centrifuged (5 min, 300 g, 4°C) then 2 ml digestion medium was added to the digestion tube and incubated at 37°C with regular mixing. After 10 min, the digestion medium was robustly mixed with a 1 ml pipette. Upon settlement of large fragments, medium with cells was transferred to the previous collection tube with new FACS-buffer and centrifuged (5 min, 300 g, 4°C). Again, 2 ml digestion medium was added to the digestion tube and the mixture was robustly mixed every 5 min until all remaining fragments were digested.

Differentiation assays

For adipogenesis, 2×10^5 cells/well in a 6-well plate were incubated with DMEM supplemented with 10% fetal calf serum (FCS), 1% antibiotics (Gibco Penicillin-Streptomycin, Thermo Fisher), 1 μ M dexamethasone (Sigma-Aldrich), 0.1 mM indomethacin (Sigma-Aldrich), 0.5 mM 3-isobutyl-1-methylxanthine (IBMX, Sigma-Aldrich) and 10 μ M insulin (Sigma-Aldrich). Medium was replaced twice per week for 3 weeks, after which the cells were fixed with 10% formaldehyde for 20 min at room temperature and stained with Oil Red O (Sigma-Aldrich). For chondrogenesis, 4×10^5 cells were pelleted in a 15 ml tube and cultured in DMEM supplemented with 1% antibiotics (Gibco Penicillin-Streptomycin, Thermo Fisher), ITS-premix (BD Biosciences), 0.1 μ M dexamethasone, 86.5 μ M L-ascorbic acid 2-phosphate (Sigma-Aldrich) and 10 ng/ml TGF β 1 (Peprotech). For microscopy, pellets were sectioned and stained for 10 min with 0.2% Toluidine Blue. For osteogenesis, 50×10^3 cells/well were cultured in a 6-well plate with DMEM supplemented with 10% FCS, 1% antibiotics (Gibco Penicillin-Streptomycin, Thermo Fisher), 0.1 μ M dexamethasone, 10 mM β -glycerophosphate (Sigma-Aldrich) and 173 μ M L-ascorbic acid 2-phosphate. Cells were fixed for 15 min in 10% formaldehyde and subsequently stained with Alizarin Red S (20 mg/ml, BDH).

In vitro stimulation and mRNA transcript analysis

To determine transcript levels, 1×10^5 mesenchymal cells were seeded in 24-well plates and allowed to adhere for 2-4 h in 1:1 (vol/vol) MesenCult proliferation medium (STEMCELL Technologies) and DMEM-F12 medium supplemented with 10% FCS and 2% antibiotics with glutamine. After 2-4 h, medium was replaced with DMEM-F12, 5% FCS with 2% antibiotics and glutamine. The next day, stimulations with retinoic acid or agonistic anti-LT β R monoclonal antibody (mAb) were performed in DMEM-F12, 2% FCS with 2% antibiotics and glutamine. For sequential stimulation experiments, cells were cultured for 6 h either in medium alone or in the presence of retinoic acid (100 nM Fluka, Sigma-Aldrich, dissolved in ethanol), after which the cells were washed and stimulated with or without agonistic anti-LT β R mAb for another 6 h (2 μ g/ml, clone 4H8-WH2, produced in the laboratory of C.F.W. and commercially available). Cells were subsequently lysed, after which mRNA was isolated from total RNA using the mRNA Capture Kit (Roche) and cDNA was synthesized using the Reverse Transcriptase Kit (Promega Benelux) according to the manufacturer's protocol.

To determine transcript levels within whole-mount lymph nodes, lymph nodes were harvested, lysed and homogenized in TRIzol Reagent (Life Technologies). RNA was isolated by precipitation with isopropanol according to the manufacturer's protocol and cDNA was synthesized from total RNA using RevertAid First Strand cDNA Synthesis Kit (Fermentas Life Sciences) according to the manufacturer's protocol.

Quantitative RT-PCR was performed on an ABI Prism 7900HT Sequence Detection System (PE Applied Biosystems) or StepOnePlus Real-Time PCR System (Thermo Fisher Scientific). Total volume of the reaction mixture was 10 μ l, containing cDNA, 300 nM of each primer and SYBR Green Mastermix (PE Applied Biosystems). From a set of eight housekeeping genes, the two most stable were selected (*Ppia* and *Hprt*). The comparative Ct method (Δ Ct) was used to indicate relative changes in mRNA levels between samples. Relative mRNA levels of unstimulated cells or control tissues were set at 1.0. Primers are listed in Table S1.

Flow cytometric analysis

To determine cell surface expression, 1×10^5 cells were cultured as indicated. Cells were stimulated with retinoic acid (100 nM), the agonistic anti-LT β R mAb or both for 24 h and 72 h. Cells were harvested by trypsinization and subsequently stained with biotin conjugated anti-VCAM-1 or anti-ICAM-1

(both eBioscience, Immunosource; 1/100), unlabeled anti-MAdCAM-1 [clone MECA 367, affinity purified from hybridoma cell culture supernatants with Pierce protein G-agarose (20398, Thermo Fisher Scientific), produced by the Monoclonal Antibody Facility, Amsterdam UMC, The Netherlands (hereafter MO2Ab Facility); 1/100] and unlabeled anti-LT β R mAb and subsequently counterstained with streptavidin-Alexa 488 and goat-anti-rat-Alexa 488 (all Invitrogen; 1/400), respectively. Sytox Blue (Invitrogen; 1/10,000) staining was used to discriminate between live and dead cells. Data were acquired on a Cyan ADP High Performance Research Flow Cytometer (Beckman Coulter) and were analyzed with Summit Software v4.3.

For flow cytometric cell sorting, lymph node single-cell suspensions were incubated with anti-mouse CD45 Pacific Orange (Thermo Fisher, clone 30-F11, 1/200), Brilliant Violet 605 anti-mouse TER-119, Alexa Fluor 488 anti-mouse podoplanin (clone 8.1.1., 1/200), PE anti-mouse CD11c (clone N418, 1/400), PE-Cy7 anti-mouse CD31 (clone 390; 1/300) (all BioLegend) and Alexa Fluor 647 anti-mouse MHC-II (clone M5/114, MO2Ab Facility). Cell sorting was performed on a MoFlo High Speed Cell Sorter (DakoCytomation) equipped with Summit Software or a BD FACSAria Fusion (BD Biosciences) using a 100- μ m nozzle.

RelB translocation and TransAM-analysis

Nuclear translocation of RelB was determined on cytopspins of cells stimulated for 6 h with retinoic acid followed by agonistic anti-LT β R mAb stimulation for 6 h. Cells were fixed with 4% paraformaldehyde (Electron Microscopy Sciences) for 5 min and subsequently permeabilized with 0.2% Triton X-100 and stained with anti-RelB (4954S, Cell Signaling Technology; 1/50) followed by Alexa Fluor 546-conjugated goat anti-rabbit IgG (A-11010, Jackson ImmunoResearch; 1/200). Cells were embedded in Vinol mounting media (Air Products) supplemented with DAPI (Invitrogen; 1/10,000) to visualize nuclei. Analysis was performed on a Leica DM6000 fluorescence microscope (Leica Microsystems) equipped with LAS AF software.

For TransAM analysis, cells were stimulated for 6 h with retinoic acid (100 nM), followed by 3 h stimulation with the agonistic anti-LT β R mAb, after which nuclear extracts were prepared with the NucBuster Protein Extraction Kit (Thermo Scientific) according to the manufacturer's protocol. DNA-binding capacity of the Nf- κ B subunits RelB and p52 was determined with the Nf- κ B TransAM Family Kit (Active Motif) according to the manufacturer's protocol.

Fluorescence in situ hybridization

Lymph nodes were fixed for 2 h in 4% paraformaldehyde at room temperature. Samples were cryoprotected and subsequently embedded in OCT compound (Sakura Finetek) and stored at -80°C until sectioning all under RNase-free conditions. Cryostat sections (7 μ m) were collected on SuperFrost Plus adhesive slides (VWR). For each target mRNA, we purchased a kit containing a DNA probe set, a DNA HCR amplifier, and hybridization, wash and amplification buffers, and multiplex *in situ* hybridizations were performed according to the manufacturer's protocol (Molecular Instruments; Choi et al., 2018). In short, slides were washed with $5 \times$ SSCT, then pre-hybridized in hybridization buffer, at 37°C in a humidified chamber. Probes were added at 0.4 pmol/100 μ l in probe hybridization buffer at 37°C and hybridized overnight in a humidified chamber, covered with parafilm. The following day, slides were washed in decreasing concentrations of probe wash buffer in $5 \times$ SSCT (100%, 75%, 50%, 25%, respectively) and washed in $5 \times$ SSCT at room temperature. Next, samples were pre-incubated with amplification buffer for 30 min. Hairpin solutions were prepared with 6 pmol snap-cooled hairpins/100 μ l and added to the slides. Samples were incubated overnight at room temperature in a humidified chamber. The following day, excess hairpins were removed by washing with $5 \times$ SSCT. In case of additional antibody staining, antibodies and/or nuclear labeling were added during these washing steps. Finally, slides were embedded in mounting medium and stored at 4°C until analysis.

Immunofluorescence

Lymph nodes (from animals 0-6 weeks of age) and spleens from C57BL/6 J and Nes-CRE^{ERT2} \times DN RAR 403 mice were fixed in 4% formaldehyde for

10 min. Samples were cryoprotected and subsequently embedded in OCT compound (Sakura Finetek) and stored at -80°C until sectioning. Cryostat sections ($7\ \mu\text{m}$) collected on gelatin-coated glasses were fixed in ice-cold acetone for 10 min and blocked with 10% normal mouse serum in PBS prior to antibody staining. Immunofluorescence staining was performed in PBS, supplemented with 0.1% (wt/vol) bovine serum albumin.

Sections were embedded in Vinol+DAPI (1/10,000) and analyzed on a Leica SP8 confocal laser scanning microscope or a Leica DM6000 (both Leica Microsystems).

For whole-mount immunofluorescence, lymph nodes were fixed in 4% formaldehyde for 10 min, washed with PBS, dehydrated with a methanol series (50%, 75%, 95%, 100% twice) and subsequently rehydrated. Lymph nodes were blocked with PBS-MT (1% skimmed milk, 0.4% Triton X-100) overnight at 4°C and subsequently incubated with directly labeled primary antibody for 4 days in PBS-MT, 4°C , with rolling. After three washing steps in PBS, lymph nodes were embedded in 1.5% low-melting agarose for ease of handling. Samples were dehydrated with a methanol series (50%, 75%, 95%, 100%, 100%) and incubated overnight in 1:1 methanol:BABB (benzylalcohol-benzylbenzoate 1:2, both Sigma-Aldrich). Next morning, all solutions were replaced with BABB and stored in the dark until acquisition. Acquisition was performed using an Ultramicroscope (La Vision BioTec). Images were analyzed using Imaris Software (Bitplane, version 8.02 or higher).

For volumetric analysis of B-cell follicles and lymph node size, individual B-cell follicles as well as the whole lymph node were masked in Imaris Software and volumes were extracted using Imaris Vantage module. The ratio of B-cell follicles to total lymph nodes was calculated as the total volume of B-cell follicles within the lymph node volume.

The following anti-mouse antibodies were used: anti-Aldh1a1 (ab23375, Abcam; 1/100) (van de Pavert et al., 2014), biotinylated anti-CXCL13 (BAF470, R&D Systems, 1/100), Alexa Fluor 488-labeled anti-B220 (clone 6B2, MO2Ab Facility, 1/300), anti-MAdCAM-1 (clone MECA367, MO2Ab Facility, 1/400), anti-CD4 (clone GK1.5 1/400), Alexa Fluor 555-labeled anti-CD4 (clone GK1.5, MO2Ab Facility, 1/400), BV510 and Alexa Fluor 647-labeled anti-CD35 (clone 8C12, BD Biosciences; 1/100), anti-CD31 (clone ERMP12, MO2Ab Facility, 1/300) and eFluor 660-labeled anti-Tyve1 (clone Aly7, eBioscience; 1/100). Unconjugated anti-Aldh1a1 was detected with Alexa Fluor 546-conjugated goat anti-rabbit IgG (A-11010, Jackson ImmunoResearch; 1/400). Biotinylated anti-CXCL13 was visualized with signal amplification using a TSA Kit with HRP-streptavidin and Alexa Fluor 546 tyramide (Invitrogen) according to the manufacturer's protocol. Clones GK1.5, ERMP12, 6B2 and MECA-367 were affinity purified from hybridoma cell culture supernatants with Pierce protein G-agarose (20398, Thermo Fisher Scientific). Antibodies were fluorescently labeled using the Alexa Fluor 488 antibody labeling kit (A20181, Invitrogen; clones GK1.5, 6B2, MECA367), Alexa Fluor 555 labeling kit (A20187, Invitrogen; clones GK1.5, MECA367) or Alexa Fluor 647 labeling kit (A20186, Invitrogen; ERMP12), all according to manufacturer's instructions. All clones are commercially available.

Statistical analysis

Statistical analysis was performed as described in the figure legends.

Competing interests

The authors declare no competing or financial interests.

Author contributions

Conceptualization: J.J.K., R.M.R., E.C.B., R.E.M.; Methodology: J.J.K., A.R., R.M.R., T.K., J.P., R.E.M.; Validation: J.J.K.; Formal analysis: J.J.K.; Investigation: J.J.K.; Resources: J.P., C.F.W., E.C.B.; Writing - original draft: J.J.K.; Writing - review & editing: J.J.K., R.E.M.; Visualization: J.J.K.; Supervision: E.C.B., R.E.M.; Funding acquisition: J.J.K., R.E.M.

Funding

This work was supported by National Institutes of Health grants (R01-AI130471, R01 CA228019 and R37-AI047822), a MERIT award from the U.S. Department of Veterans Affairs (101 BX-789 002919 to E.C.B.) and a Netherlands Organization for Scientific Research (Nederlandse Organisatie voor Wetenschappelijk Onderzoek) grant (ALWOP.271 to J.J.K.). Deposited in PMC for release after 12 months.

Peer review history

The peer review history is available online at <https://journals.biologists.com/dev/article-lookup/doi/10.1242/dev.199713>

References

- Ahrendt, M., Hammerschmidt, S. I., Pabst, O., Pabst, R. and Bode, U. (2008). Stromal cells confer lymph node-specific properties by shaping a unique microenvironment influencing local immune responses. *J. Immunol.* **181**, 1898-1907. doi:10.4049/jimmunol.181.3.1898
- Austana, L. M. I., Carlsen, H., Ertesvag, A., Alexander, G., Blomhoff, H. K. and Blomhoff, R. (2004). Vitamin A status significantly alters nuclear factor- κ B activity assessed by in vivo imaging. *FASEB J.* **18**, 1255-1257. doi:10.1096/fj.03-1098fj
- Baptista, A. P., Roozendaal, R., Reijmers, R. M., Koning, J. J., Unger, W. W., Greuter, M., Keuning, E. D., Molenaar, R., Goverse, G., Sneeboer, M. M. et al. (2014). Lymph node stromal cells constrain immunity via MHC class II self-antigen presentation. *eLife* **3**, e04433. doi:10.7554/eLife.04433
- Baptista, A. P., Gola, A., Huang, Y., Milanez-Almeida, P., Torabi-Parizi, P., Urban, J. F., Jr., Shapiro, V. S., Gerner, M. Y. and Germain, R. N. (2019). The chemoattractant receptor Ebi2 drives intranodal naive CD4⁺ T cell peripheralization to promote effective adaptive immunity. *Immunity*, **50**, 1188-201.e6. doi:10.1016/j.immuni.2019.04.001
- Bovay, E., Sabine, A., Prat-Luri, B., Kim, S., Son, K., Willrodt, A.-H., Olsson, C., Halin, C., Kiefer, F., Betsholtz, C. et al. (2018). Multiple roles of lymphatic vessels in peripheral lymph node development. *J. Exp. Med.* **215**, 2760-2777. doi:10.1084/jem.20180217
- Castagnaro, L., Lenti, E., Maruzzelli, S., Spinardi, L., Migliori, E., Farinello, D., Sitia, G., Harrelson, Z., Evans, S. M., Guidotti, L. G. et al. (2013). Nkx2-5⁺islet1⁺ mesenchymal precursors generate distinct spleen stromal cell subsets and participate in restoring stromal network integrity. *Immunity* **38**, 782-791. doi:10.1016/j.immuni.2012.12.005
- Chai, Q., Onder, L., Scandella, E., Gil-Cruz, C., Perez-Shibayama, C., Cupovic, J., Danuser, R., Sparwasser, T., Luther, S. A., Thiel, V. et al. (2013). Maturation of lymph node fibroblastic reticular cells from myofibroblastic precursors is critical for antiviral immunity. *Immunity* **38**, 1013-1024. doi:10.1016/j.immuni.2013.03.012
- Chang, J. E. and Turley, S. J. (2015). Stromal infrastructure of the lymph node and coordination of immunity. *Trends Immunol.* **36**, 30-39. doi:10.1016/j.it.2014.11.003
- Choi, H. M. T., Schwarzkopf, M., Fornace, M. E., Acharya, A., Artavanis, G., Stegmaier, J., Cunha, A. and Pierce, N. A. (2018). Third-generation in situ hybridization chain reaction: multiplexed, quantitative, sensitive, versatile, robust. *Development* **145**, dev165753. Retrieved from doi:10.1242/dev.165753. <https://www.ncbi.nlm.nih.gov/pubmed/29945988>
- Crowe, P. D., Vanarsdale, T. L., Walter, B. N., Ware, C. F., Hession, C., Ehrenfels, B., Browning, J. L., Din, W. S., Goodwin, R. G. and Smith, C. A. (1994). A lymphotoxin-beta-specific receptor. *Science* **264**, 707-710. doi:10.1126/science.8171323
- Cupedo, T., Jansen, W., Kraal, G. and Mebius, R. E. (2004). Induction of secondary and tertiary lymphoid structures in the skin. *Immunity* **21**, 655-667. doi:10.1016/j.immuni.2004.09.006
- Dejardin, E., Droin, N. M., Delhase, M., Haas, E., Cao, Y., Makris, C., Li, Z.-W., Karin, M., Ware, C. F. and Green, D. R. (2002). The lymphotoxin- β receptor induces different patterns of gene expression via two NF- κ B pathways. *Immunity* **17**, 525-535. doi:10.1016/S1074-7613(02)00423-5
- Endres, R., Alimzhanov, M. B., Plitz, T., Fütterer, A., Kosco-Vilbois, M. H., Nedospasov, S. A., Rajewsky, K. and Pfeffer, K. (1999). Mature follicular dendritic cell networks depend on expression of lymphotoxin β receptor by radioresistant stromal cells and of lymphotoxin β and tumor necrosis factor by B cells. *J. Exp. Med.* **189**, 159-168. doi:10.1084/jem.189.1.159
- Fletcher, A. L., Lukacs-Kornek, V., Reynoso, E. D., Pinner, S. E., Bellemare-Pelletier, A., Curry, M. S., Collier, A.-R., Boyd, R. L. and Turley, S. J. (2010). Lymph node fibroblastic reticular cells directly present peripheral tissue antigen under steady-state and inflammatory conditions. *J. Exp. Med.* **207**, 689-697. doi:10.1084/jem.20092642
- Fu, Y.-X., Huang, G., Wang, Y. and Chaplin, D. D. (1998). B lymphocytes induce the formation of follicular dendritic cell clusters in a lymphotoxin α -dependent fashion. *J. Exp. Med.* **187**, 1009-1018. doi:10.1084/jem.187.7.1009
- Hammerschmidt, S. I., Ahrendt, M., Bode, U., Wahl, B., Kremmer, E., Förster, R. and Pabst, O. (2008). Stromal mesenteric lymph node cells are essential for the generation of gut-homing T cells in vivo. *J. Exp. Med.* **205**, 2483-2490. doi:10.1084/jem.20080039
- Honda, K., Nakano, H., Yoshida, H., Nishikawa, S., Rennert, P., Ikuta, K., Tamechika, M., Yamaguchi, K., Fukumoto, T., Chiba, T. et al. (2001). Molecular basis for hematopoietic/mesenchymal interaction during initiation of Peyer's patch organogenesis. *J. Exp. Med.* **193**, 621-630. doi:10.1084/jem.193.5.621
- Hoorweg, K., Narang, P., Li, Z., Thuery, A., Papazian, N., Withers, D. R., Coles, M. C. and Cupedo, T. (2015). A stromal cell niche for human and mouse

- type 3 innate lymphoid cells. *J. Immunol.* **195**, 4257-4263. doi:10.4049/jimmunol.1402584
- Imayoshi, I., Ohtsuka, T., Metzger, D., Chambon, P. and Kageyama, R. (2006). Temporal regulation of Cre recombinase activity in neural stem cells. *Genesis* **44**, 233-238. doi:10.1002/dvg.20212
- Jarjour, M., Jorquera, A., Mondor, I., Wienert, S., Narang, P., Coles, M. C., Klauschen, F. and Bajénoff, M. (2014). Fate mapping reveals origin and dynamics of lymph node follicular dendritic cells. *J. Exp. Med.* **211**, 1109-1122. doi:10.1084/jem.20132409
- Katakai, T., Hara, T., Lee, J.-H., Gonda, H., Sugai, M. and Shimizu, A. (2004). A novel reticular stromal structure in lymph node cortex: an immuno-platform for interactions among dendritic cells, T cells and B cells. *Int. Immunol.* **16**, 1133-1142. doi:10.1093/intimm/dxh113
- Kedishvili, N. Y. (2016). Retinoic acid synthesis and degradation. *Subcell. Biochem.* **81**, 127-161. Retrieved from. doi:10.1007/978-94-024-0945-1_5. <https://www.ncbi.nlm.nih.gov/pubmed/27830503>
- Koning, J. J. and Mebius, R. E. (2012). Interdependence of stromal and immune cells for lymph node function. *Trends Immunol.* **33**, 264-270. doi:10.1016/j.it.2011.10.006
- Koning, J. J., Konijn, T., Lakeman, K. A., O'Toole, T., Kenswil, K. J. G., Raaijmakers, M. H. G. P., Michurina, T. V., Enikolopov, G. and Mebius, R. E. (2016). Nestin-expressing precursors give rise to both endothelial as well as nonendothelial Lymph node stromal cells. *J. Immunol.* **197**, 2686-2694. doi:10.4049/jimmunol.1501162
- Krautler, N. J., Kana, V., Kranich, J., Tian, Y., Perera, D., Lemm, D., Schwarz, P., Armulik, A., Browning, J. L., Tallquist, M. et al. (2012). Follicular dendritic cells emerge from ubiquitous perivascular precursors. *Cell* **150**, 194-206. doi:10.1016/j.cell.2012.05.032
- Krishnamurthy, A. T. and Turley, S. J. (2020). Lymph node stromal cells: cartographers of the immune system. *Nat. Immunol.* **21**, 369-380. doi:10.1038/s41590-020-0635-3
- Lee, J.-W., Epardaud, M., Sun, J., Becker, J. E., Cheng, A. C., Yonekura, A.-r., Heath, J. K. and Turley, S. J. (2007). Peripheral antigen display by lymph node stroma promotes T cell tolerance to intestinal self. *Nat. Immunol.* **8**, 181-190. doi:10.1038/ni1427
- Link, A., Vogt, T. K., Favre, S., Britschgi, M. R., Acha-Orbea, H., Hinz, B., Cyster, J. G. and Luther, S. A. (2007). Fibroblastic reticular cells in lymph nodes regulate the homeostasis of naive T cells. *Nat. Immunol.* **8**, 1255-1265. doi:10.1038/ni1513
- Magnusson, F. C., Liblaur, R. S., von Boehmer, H., Pittet, M. J., Lee, J. W., Turley, S. J. and Khazaie, K. (2008). Direct presentation of antigen by lymph node stromal cells protects against CD8 T-cell-mediated intestinal autoimmunity. *Gastroenterology* **134**, 1028-1037. doi:10.1053/j.gastro.2008.01.070
- Mebius, R. E. (2003). Organogenesis of lymphoid tissues. *Nat. Rev. Immunol.* **3**, 292-303. doi:10.1038/nri1054
- Mitchell, J. and Abbot, A. (1965). Ultrastructure of the antigen-retaining reticulum of lymph node follicles as shown by high-resolution autoradiography. *Nature* **208**, 500-502. doi:10.1038/208500b0
- Mizee, M. R., Wooldrik, D., Lakeman, K. A. M., van het Hof, B., Drexhage, J. A. R., Geerts, D., Bugiani, M., Aronica, E., Mebius, R. E., Prat, A. et al. (2013). Retinoic acid induces blood-brain barrier development. *J. Neurosci.* **33**, 1660-1671. doi:10.1523/JNEUROSCI.1338-12.2013
- Molenaar, R., Greuter, M., van der Marel, A. P. J., Roozendaal, R., Martin, S. F., Edele, F., Huehn, J., Förster, R., O'Toole, T., Jansen, W. et al. (2009). Lymph node stromal cells support dendritic cell-induced gut-homing of T cells. *J. Immunol.* **183**, 6395-6402. doi:10.4049/jimmunol.0900311
- Molenaar, R., Knippenberg, M., Goverse, G., Olivier, B. J., de Vos, A. F., O'Toole, T. and Mebius, R. E. (2011). Expression of retinaldehyde dehydrogenase enzymes in mucosal dendritic cells and gut-draining lymph node stromal cells is controlled by dietary vitamin A. *J. Immunol.* **186**, 1934-1942. doi:10.4049/jimmunol.1001672
- Mueller, S. N. and Germain, R. N. (2009). Stromal cell contributions to the homeostasis and functionality of the immune system. *Nat. Rev. Immunol.* **9**, 618-629. doi:10.1038/nri2588
- Nichols, L. A., Chen, Y., Colella, T. A., Bennett, C. L., Clausen, B. E. and Engelhard, V. H. (2007). Deletional self-tolerance to a melanocyte/melanoma antigen derived from tyrosinase is mediated by a radio-resistant cell in peripheral and mesenteric lymph nodes. *J. Immunol.* **179**, 993-1003. doi:10.4049/jimmunol.179.2.993
- Onder, L., Mörbé, U., Pikor, N., Novkovic, M., Cheng, H.-W., Hehlgans, T., Pfeffer, K., Becher, B., Waisman, A., Rüllicke, T. et al. (2017). Lymphatic endothelial cells control initiation of lymph node organogenesis. *Immunity* **47**, 80-92.e4. doi:10.1016/j.immuni.2017.05.008
- Rajaii, F., Bitzer, Z. T., Xu, Q. and Sockanathan, S. (2008). Expression of the dominant negative retinoid receptor, RAR403, alters telencephalic progenitor proliferation, survival, and cell fate specification. *Dev. Biol.* **316**, 371-382. doi:10.1016/j.ydbio.2008.01.041
- Rodda, L. B., Lu, E., Bennett, M. L., Sokol, C. L., Wang, X., Luther, S. A., Barres, B. A., Luster, A. D., Ye, C. J. and Cyster, J. G. (2018). Single-cell RNA sequencing of Lymph node stromal cells reveals niche-associated heterogeneity. *Immunity* **48**, 1014-1028.e6. doi:10.1016/j.immuni.2018.04.006
- Roozendaal, R. and Mebius, R. E. (2011). Stromal cell-immune cell interactions. *Annu. Rev. Immunol.* **29**, 23-43. doi:10.1146/annurev-immunol-031210-101357
- Siebenlist, U., Franzoso, G. and Brown, K. (1994). Structure, regulation and function of NF- κ B. *Annu. Rev. Cell Biol.* **10**, 405-455. doi:10.1146/annurev.cb.10.110194.002201
- Suzuki, K., Maruya, M., Kawamoto, S., Sitnik, K., Kitamura, H., Agace, W. W. and Fagarasan, S. (2010). The sensing of environmental stimuli by follicular dendritic cells promotes immunoglobulin A generation in the gut. *Immunity* **33**, 71-83. doi:10.1016/j.immuni.2010.07.003
- Takada, K. and Jameson, S. C. (2009). Naive T cell homeostasis: from awareness of space to a sense of place. *Nat. Rev. Immunol.* **9**, 823-832. doi:10.1038/nri2657
- van de Pavert, S. A., Olivier, B. J., Goverse, G., Vondenhoff, M. F., Greuter, M., Beke, P., Kusser, K., Höpken, U. E., Lipp, M., Niederreither, K. et al. (2009). Chemokine CXCL13 is essential for lymph node initiation and is induced by retinoic acid and neuronal stimulation. *Nat. Immunol.* **10**, 1193-1199. doi:10.1038/ni.1789
- van de Pavert, S. A., Ferreira, M., Domingues, R. G., Ribeiro, H., Molenaar, R., Moreira-Santos, L., Almeida, F. F., Ibiza, S., Barbosa, I., Goverse, G. et al. (2014). Maternal retinoids control type 3 innate lymphoid cells and set the offspring immunity. *Nature* **508**, 123-127. doi:10.1038/nature13158
- Vondenhoff, M. F., Greuter, M., Goverse, G., Elewaut, D., Dewint, P., Ware, C. F., Hoorweg, K., Kraal, G. and Mebius, R. E. (2009). LT β R signaling induces cytokine expression and up-regulates lymphangiogenic factors in lymph node anlagen. *J. Immunol.* **182**, 5439-5445. doi:10.4049/jimmunol.0801165
- Wolters, D. A., Coenen-de Roo, C. J., Mebius, R. E., van der Cammen, M. J., Tirion, F., Miltenburg, A. M. and Kraal, G. (1999). Intranasally induced immunological tolerance is determined by characteristics of the draining lymph nodes: studies with OVA and human cartilage gp-39. *J. Immunol.* **162**, 1994-1998.
- Yip, L., Su, L., Sheng, D., Chang, P., Atkinson, M., Czesak, M., Albert, P. R., Collier, A.-R., Turley, S. J., Fathman, C. G. et al. (2009). Deaf1 isoforms control the expression of genes encoding peripheral tissue antigens in the pancreatic lymph nodes during type 1 diabetes. *Nat. Immunol.* **10**, 1026-1033. doi:10.1038/ni.1773
- Zhang, Z., Li, J., Zheng, W., Zhao, G., Zhang, H., Wang, X., Guo, Y., Qin, C. and Shi, Y. (2016). Peripheral lymphoid volume expansion and maintenance are controlled by gut microbiota via RALDH+ dendritic cells. *Immunity* **44**, 330-342. doi:10.1016/j.immuni.2016.01.004

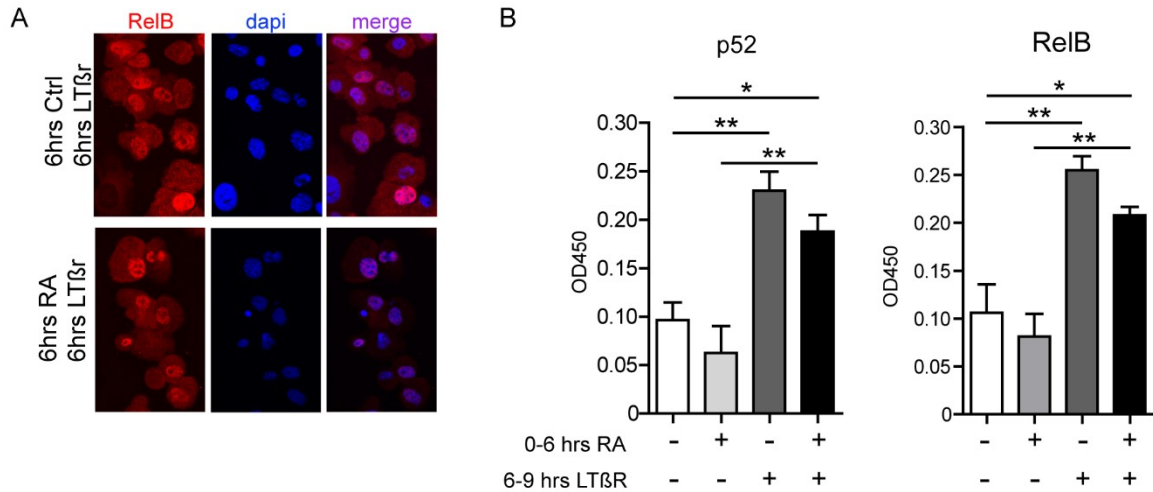


Fig. S1. Related to Figure 1. Retinoic Acid signaling prevents upregulation of FRC related genes
 (A) Immunofluorescence staining for RelB (in red) and nuclei (in blue) in cytoplasts of mesenchymal precursors stimulated with or without retinoic acid (6hrs) followed by agonistic anti-LTβR mAb (6hrs). B) TransAM analysis of nuclear p52 and relB after stimulation of mesenchymal precursors with retinoic acid (6hrs) followed by agonistic anti-LTβR mAb (3hrs) or retinoic acid (6hrs) alone or anti-LTβR mAb (3hrs) alone. Results are representative of 3 independent experiments. The data represent mean ± SEM; n = 3, * p < 0.05, ** p < 0.01, one-way ANOVA with Bonferroni's multiple comparison test.

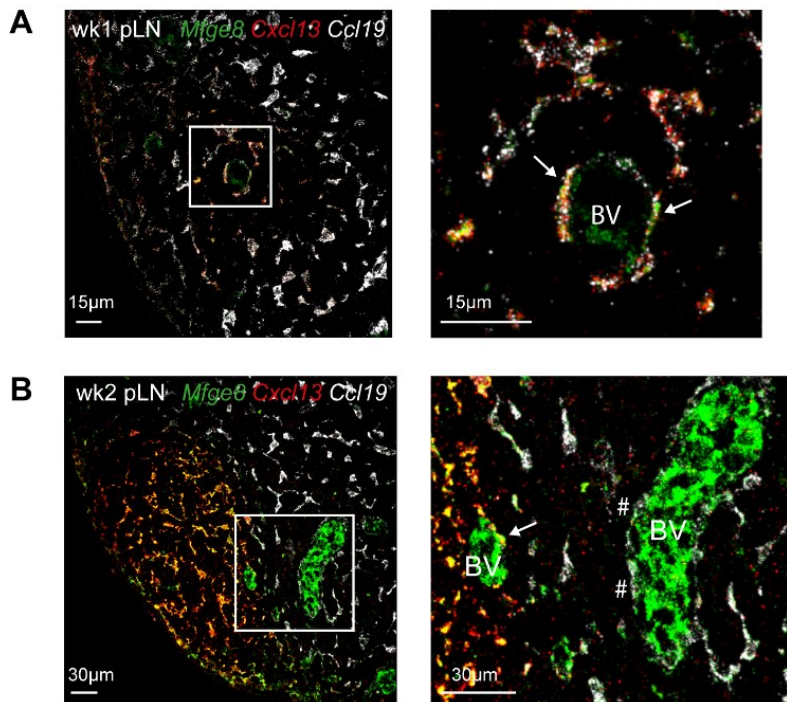


Fig. S2. Related to Figure 2 Localization of FDC precursors

A-B) Confocal analysis of peripheral lymph nodes (pLN) by multiple fluorescence *in situ* hybridizations at different timepoints after birth. A) Combined expression of *Mfge8*, *Cxcl13* and *Ccl19* in peripheral lymph nodes at 1 week after birth. Arrows indicate cells around blood vessel (BV) expressing *Mfge8*, *Cxcl13* and *Ccl19*. B) Combined expression of *Mfge8*, *Cxcl13* and *Ccl19* in lymph nodes at 2 weeks after birth. Arrows indicate cells around blood vessel (BV) that express *Mfge8* and *Cxcl13*, hashtags indicate cells around blood vessel (BV) that express *Mfge8* and *Ccl19*. The data represent n = 3.

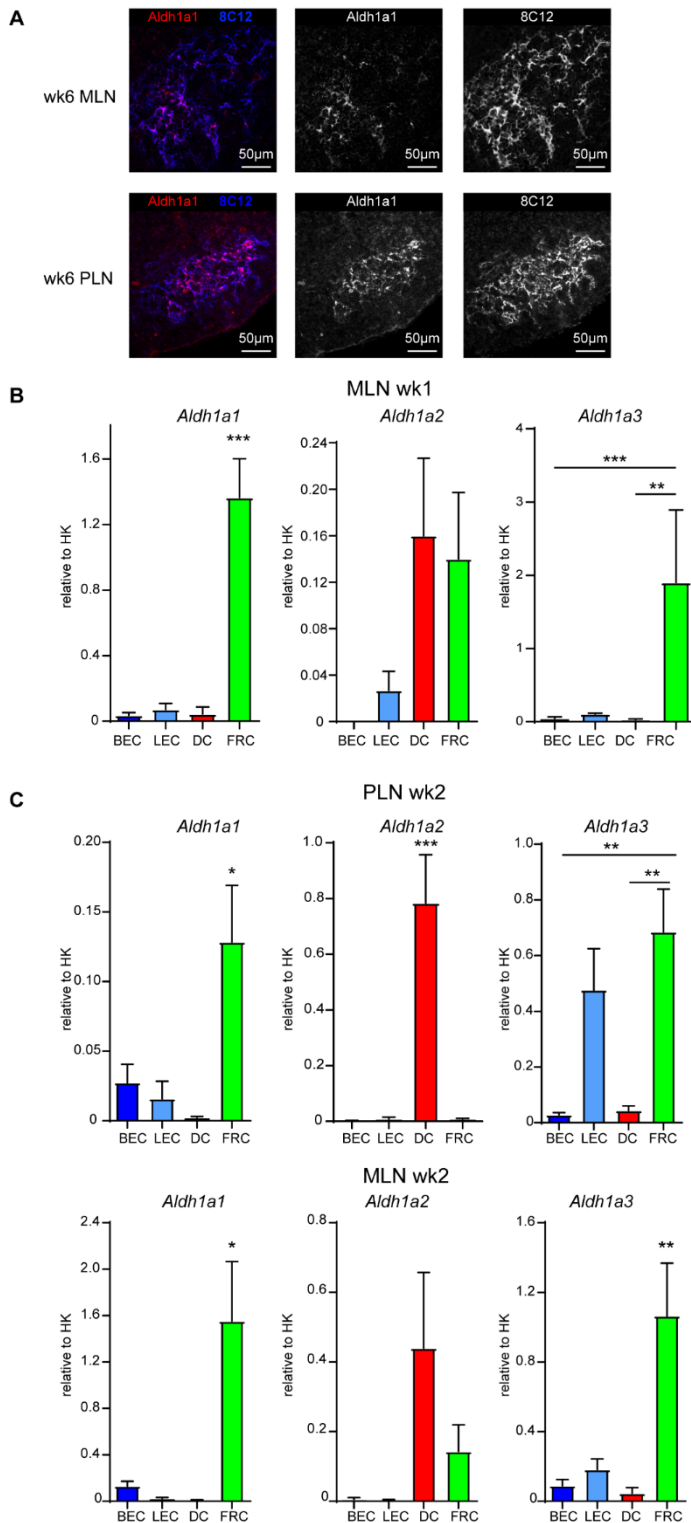


Fig. S3. Related to figure 3 Multiple cellular sources of Aldh1 enzymes

mRNA expression levels of *Aldh1a1-3* enzymes relative to housekeeping genes in sorted stromal cells and dendritic cells of peripheral lymph nodes (pLN) or mesenteric lymph nodes (mLN) at the indicated timepoints. The data represent mean \pm SEM; n = 3.

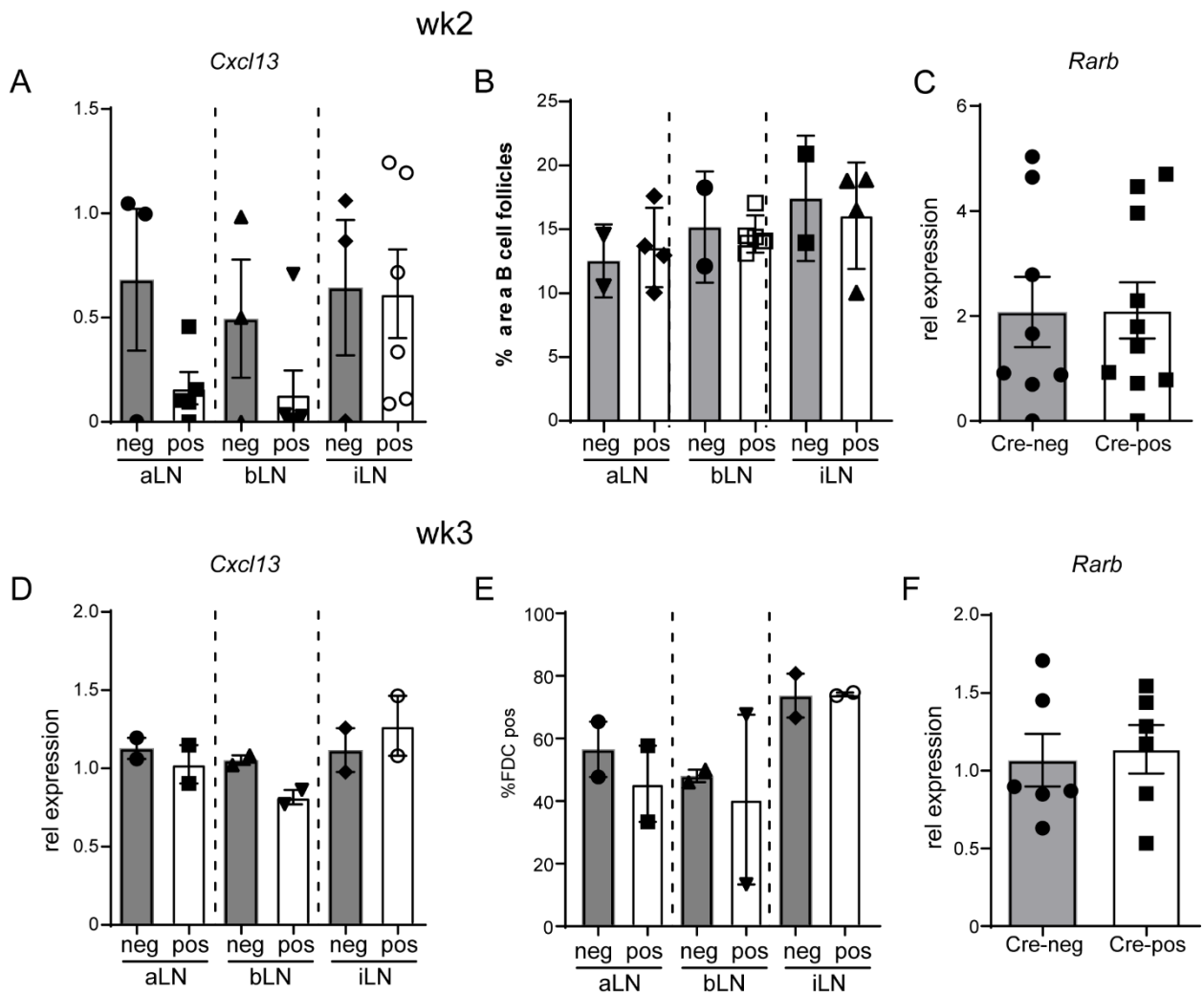


Fig. S4. Related to figure 4. *RAR* signaling blockade in nestin precursors does not prevent FDC formation.

A and D) Relative *Cxcl13* mRNA expression in indicated peripheral lymph nodes (pLN) of in 2-week-old (A) and in 3-week-old (D) Nes-Cre^{ERT2pos} x DN-RAR mice compared to Nes-Cre^{ERT2neg} x DN-RAR littermates. B) Quantification of B-cell areas in 2-week-old Nes-Cre^{ERT2pos} x DN-RAR mice compared to Nes-Cre^{ERT2neg} x DN-RAR littermates. C and F) Relative *Rarb* mRNA expression in pLN of 2-week-old (C) and 3-week-old (E) Nes-Cre^{pos}xRarDN mice compared with Nes-Cre^{neg}xRarDN littermates. E) Quantification of %FDC pos B-cell follicles in 3-week-old Nes-Cre^{ERT2pos} x DN-RAR mice compared to Nes-Cre^{ERT2neg} x DN-RAR littermates. The data represent mean \pm SEM; n = 2 or more.

Fig. S5. Related to Figure 5. Inhibiting retinoic acid receptor signaling prevents CXCL13 expression and development of FDCs in lymph nodes A-C) Immunofluorescence staining for B cells (green) and T cells (red) in peripheral and mesenteric lymph nodes of vehicle treated (DMSO) and BMS493 treated animals. D) Heatmap showing mRNA expression levels of listed genes in mesenteric lymph nodes upon treatment for 7 and 10 days with BMS493, starting at day 4 after birth. E) Quantification of the number of B cell follicles in DMSO and BMS493 treated animals in both peripheral and mesenteric lymph nodes. F) mRNA expression levels of *Rarb* and *Cxcl13* in spleen upon treatment with vehicle (DMSO) or BMS493 for 7 and 10 days starting at day 4 after birth. G) Immunofluorescence analysis of FDC (8C12 in blue) network in spleen of vehicle (DMSO) or BMS493 treated animals 10 days after treatment. H) Representative ultramicroscopy image of a whole mount stained peripheral lymph node from DMSO treated mice showing B cell follicles in blue and total lymph node volume in orange. I-J) Volume of B cell follicles and whole lymph nodes of peripheral lymph nodes of mice that were treated with suboptimal dose of BMS493 vs DMSO for 14 days starting at day 4 after birth (I) or for 7 days with BMS493 vs DMSO and left untreated for 21 days (J). Results are representative of at least 3 individual mice. The data in D, E, F, I-J represent mean \pm SEM; n = 3. n.s. not significant. *, p < 0.05; ** p < 0.01, unpaired student's t test.

Table S1. Primer sequences

Sequence	Name
ATATGGGTTTCATGGGCTTG	Mfge8 fw
GAGGCTGTAAGCCACCTTGA	Mfge8 rev
CCAGTTCCCAGACGTTGATT	Clusterin fw
AGCAGGGATGAGGTGTGGAG	Clusterin rev
CGAGTCTAAGCGGGAGACAG	Igfbp3 fw
TTGTTGGCAGTCTTTTGTGC	Igfbp3 rev
ATGCGAAGACTGCTGCC	CCL19 fw
AGCGGAAGGCTTTCACGAT	CCL19 rev
GCTGCAAGAGA ACTGAACAGA CA	CCL21 fw
CGTGAACCACCCAGCTTGA	CCL21 rev
CACCCTGGTTGGAATCATAGTTG	GP38 fw
TAGGGCGAGACCTTCCAGAAA	GP38 rev
CATAGATCGGATTCAAGTTACGCC	CXCL13 fw
TCTTGGTCCAGACACAACTTCA	CXCL13 rev
GCCTGCAGAAGTGCTTTGAAGT	RAR- β fw
GCTCTGTGCATTCTGCTTT	RAR- β rev
ATC GTG CTG CTC GCA AGT T	IL-7 fw
CAC CAG TGT TTG TGT GCC TTG T	IL7 rev
CCT ATA ATG AAC ACT GGA ACC ATC TCT	LT β R fw
TCC GAT CGC TGG TGC AA	LT β R rev
GGT TAC CTC AGC AAG ACG TTG TTT	VEGF-C fw
ATG CAC CGG CAG GAA GTG	VEGF-C rev
CTG GTG CTG ACC CAT AGA AAG	MAdCAM-1 fw
GGC TCA GCA GAG GTC GTG TT	MAdCAM-1 rev
CTC CTC TCA CGG CTC TTC A	RALDH1 fw
AAT GTT TAC CAC GCC AGG AG	RALDH1 rev
TCA TCA AAA CCC TGA GGT ATT ATG C	RALDH2 fw
GGGCTCGTGTCTTGTGAAAGTAA	RALDH2 rev
GTG TGC TTC ACC AGG CAT GA	RALDH3 fw
CAC AGG GCA GGA GCC AGT T	RALDH3 rev